ABSTRACT

Title of Thesis: CHARACTERIZATION OF FOCUSED
ULTRASOUND BEAM GEOMETRIES
USING THERMOCHROMIC LIQUID
CRYSTAL FILMS

Nabid Ahmed, Master of Science, 2020

Thesis directed by: Dr. Victor Frenkel, Department of Radiology
and Nuclear Medicine, University of Maryland
School of Medicine

Focused ultrasound (FUS) applications are gaining more attention from clinicians for being able to provide effective, non-invasive treatments to almost any region of the body. In-house development of FUS devices require characterization and quality assurance methods to verify acoustic pressure fields, focal zone geometry, location, and validate proper function. Conventional techniques (hydrophones, gel phantoms) are limited by expensive and inaccessible equipment, time-consuming procedures, and use of toxic reagents. We developed a process for using thermochromic liquid crystal (TLC) films, sensors which undergo color transition when exposed to a range of specific temperatures, as a low-cost and readily adaptable characterization method for FUS transducers. A proof-of-concept experiment showed reproducibility in detecting ultrasound beams. Tests with two FUS transducers demonstrated that the technique was able to approximate axial dimensions of the focal region and depth of the focal region, characteristics that are significant in FUS treatment planning.

CHARACTERIZATION OF FOCUSED ULTRASOUND BEAM GEOMETRIES
USING THERMOCHROMIC LIQUID CRYSTAL FILMS

by

Nabid Ahmed

Thesis submitted to the Faculty of the Graduate School of the
University of Maryland, College Park, in partial fulfillment
of the requirements for the degree of
Master of Science
2020

Advisory Committee:
 Dr. Victor Frenkel, Co-Chair
 Dr. Li-Qun Zhang, Co-Chair
 Dr. Huang Chiao Huang

<u>Acknowledgements</u>

Table of Contents

List of Abbreviations

FUS: focused ultrasound
pFUS: pulsed focused ultrasound
HIFU: high-intensity focused ultrasound
TLC: thermochromic liquid crystal
CT: computed tomography
MRI: magnetic resonance imaging
US: ultrasound
MRgFUS: magnetic resonance imaging guided focused ultrasound
CNS: central nervous system
PNS: peripheral nervous system
KHz: kilohertz
MHz: megahertz
dB: decibel

List of Tables

List of Figures

Chapter 1: Background

Section 1-1: FUS: History

Ultrasound imaging and therapy takes root in the discovery of the piezoelectric effect in the late 1800s' by Paul Jacques and Pierre Curie. Their observation of how applying a mechanical deformation to a crystalline structure with no point symmetry (such as silicon dioxide or quartz) could generate an electric charge, as well as the inverse of this phenomena, formed the technical foundation of industrial and later biomedical applications [1]. This included sonar by Paul Langevin during the first World War, physiotherapy devices pioneered by Raimer Pohlman in 1938, and the introduction of real-time diagnostic imaging into obstetric medicine by Ian Donald in the 1960's [2, 3]. Simultaneously, scientists in the field were experimenting with ultrasound at relatively higher intensities on tissues and small organisms where various physical and biological effects were observed, notably lethal heating of frogs and small fishes [4].

After the discovery that ultrasound could be focused onto a small region using a concave surface, Lynn et al. used this technique to non-invasively create focal lesions in the cortical regions in felines and in the bovine liver, which would later be referred to as high intensity focused ultrasound (HIFU) [5]. Continuing on from this work, brothers William and Francis Fry developed the first experimental HIFU system tailored for neurosurgical treatments in 1942. This device was composed of 4 individual transducers and was demonstrated to create pinpoint lesions within the basal ganglia on non-human primates [6]. From then on between the 1950-90's, multidisciplinary teams including the Fry Brothers made strides in the use of HIFU for diseases in the

brain and within the body, including but not limited to the ablation of gliomas, thyroid and breast cancer, benign prostatic hyperplasia and opening the blood-brain barrier using pulsed FUS [7-9].

Despite these advancements, HIFU applications in the brain experienced a number of limitations early on that stifled its adoption. Transducers at the time were not able to transmit FUS through the intact skull plate due to the bone's effect of distorting the beam, which prevented the accurate formation of a focal region. This required a craniectomy, an invasive procedure involving the resection of a portion of the skull, to allow these initial devices to directly interface with brain tissue. Another technical limitation was lack of necessary imaging resolution on MRI and US at the time which made accurate targeting difficult. Finally, other therapies being developed for certain conditions that were less invasive (i.e. Levodopa medication for Parkinson's) took priority over FUS.

The clinical resurgence of FUS for applications in both the brain and body over the last two decades was possible through resolving the aforementioned limitation of transcranial focusing and with the refinement in MRI and US in image guided-procedures. In the 1990s, Hynynen et al. developed a hemi-spherical transducer array which used computed tomography (CT) scans of the patients skull in a treatment planning algorithm that compensated for phase aberration effects due to the skull; this eliminated the need for craniectomy, effectively making HIFU a non-invasive neurological treatment modality [10]. Thermal monitoring techniques (i.e. MR thermometry) were developed to provide critical information involving verifying target regions, providing real-time feedback throughout the procedure, and in becoming

aware of unwanted effects in non-target tissue regions [11, 12]. Clinical trials of MRgFUS thermal ablation for many different disease pathologies such as uterine fibroids, solid tumors, essential tremor and tremor-dominant Parkinson's disease (see clinical applications section) have demonstrated safe and efficacious results; many of these procedures are now FDA-approved and conducted regularly. These milestones have permitted further investigations into the other bioeffects of FUS that can be therapeutically exploited, including drug/gene delivery, thrombolysis, modulating the immune environment, sensitization for chemotherapy or radiation, peripheral nerve stimulation and regeneration.

Section 1-2: Biological Effects of FUS

Varying intensities or generation mode (continuous vs pulsed delivery) of focused ultrasound beams determines one of many FUS-induced bioeffects that can be exploited for an ever-growing set of biomedical applications. Physical interactions that attenuate the sound beam propagating into the body occur based on the sonication parameters and characteristics of the intervening tissue (skin, fat, bone, muscle); these interactions include reflection, refraction, scattering, and absorption (conversion of mechanical energy into heat) [13]. Thermal effects can be reversible (e.g. tissue hyperthermia) or irreversible (e.g. ablation). Mechanical effects that are reversible are typically elicited at low intensities using pulsed administration (e.g. enhancing membrane permeability), while irreversible mechanical effects that lead to tissue damage are at high intensities (e.g. histotripsy).

Thermal Interactions and corresponding biomedical applications

Applying high intensity (100-10,000 W/cm^2 or higher) FUS at continuous frequencies (1-10 MHz) can lead to a temperature rises above 55°C within 1 second inside the focal region, causing coagulative necrosis [1]. Lesions have an ellipsoid geometry with a diameter around 1mm and axial lengths that are 5-20 times larger [14, 15]. During procedure planning, tissues that obstruct the beam through heat absorption (bone) or reflection (hollow organs) are avoided to prevent unwanted thermal damage. HIFU ablative therapies that are currently employed in the clinic include uterine fibroids, bone metastases, prostate cancer, essential tremor and Parkinson's disease [16-19]. Indeed, many of these now FDA approved procedures have dramatically reduced the risk of complications and the need for post-procedural hospital stays. Indications for FUS ablation therapies are steadily growing, backed by clinical trials for solid tumors of the breast, liver, kidney, and other intracranial pathologies such as Alzheimer's disease [20]

Using lower intensities and pulsed application can lead to lower temperature increases on the order of 42-46°C. This effect (tissue hyperthermia) is known to increase cancer sensitivity to chemotherapeutics and radiation therapy via multiple mechanisms including prevention of DNA repair and tumor reoxygenation [21, 22]. Many clinical trials using FUS as an adjuvant therapy for radiation and chemotherapy treatment show improved outcomes for solid malignancies of the head and neck, breast, and pancreas [23].

Mechanical Interactions of FUS propagation

Notable mechanical effects of FUS include acoustic radiation forces and cavitation. Acoustic radiation force is the transfer of momentum from the sound beam to a reflecting or absorbing tissue which can displace tissue if large enough, causing strain [24]. Acoustic streaming refers to this same effect but within a fluid medium, and is used in FUS applications dealing with clot lysis and drug delivery [25, 26]. Acoustic cavitation occurs when the rarefactive components of the sound field draw gas out of the tissue, forming microbubbles which may oscillate in a stable fashion (referred to as "stable cavitation") or in an unstable fashion at higher pressure amplitudes, leading to collapse and subsequent generation of tissue damaging shockwaves ("inertial cavitation"). Alternatively, these microbubbles (US contrast agents) can be administered into the body to create the same effects.

Biomedical applications that exploit the mechanical effects of FUS are usually via pulsed FUS at low intensities (0.125-3 W/cm^2) in order to prevent unwanted irreversible thermal effects. One neurological pFUS application making significant headway is enhancing drug delivery to the brain through blood-brain barrier disruption (BBBD) [27-29]. Increased transport and retention of different drug classes (antibodies, drug-loaded liposomes, chemotherapeutics, etc.) have been exhaustively demonstrated in preclinical animal models [30-32]. In fact, recent clinical trials validating the procedural safety of BBBD in ALS, Alzheimer's, Glioblastoma, and Parkinson's patients have been successful [33-35]. Modulation of the central (CNS) and peripheral nervous system (PNS) is another neurological application of pFUS. Continuing on from Fry *et al.'s* pioneering demonstration on how FUS can reversibly inhibit the CNS, a growing number of animal and human studies have explored and validated pFUS-mediated

stimulation of neuronal pathways that regulate mood, awareness and motor functioning [36-39]. Studies on treating peripheral nerves with pFUS have shown either effects of stimulation or suppression of action potentials [40-42]. Others have demonstrated higher rates of peripheral axonal regeneration [43, 44].

Aside from the nervous system, pFUS biomedical applications in the body range from the clinically pertinent to more ancillary or cosmetic interventions. Enhanced cytotoxicity and growth inhibition of solid tumors has been noted with co-opting pFUS with drug administration [45-47]. For vascular disorders, pFUS application has been shown to treat deep venous thrombosis, enhance arterial thrombolysis, and promote reperfusion and angiogenesis in peripheral arterial disease [48-51]. In orthopedic applications, preclinical and clinical trials have shown significant improvements in bone fracture healing rates using pFUS [52, 53]. More recently, pFUS technology has even made strides in dermatological treatment and body-contouring [54, 55].

Section 1-3: FUS Principles

The purpose of this section is to provide a working understanding of the principles of focused ultrasound and its various effects on biological tissue. Sound is a longitudinal mechanical wave that applies pressure to particles within a medium (air, water, tissue, bone), causing each particle to oscillate about a fixed point. When the sound wave is at peak pressure, the molecules are in maximal compression; when at minimal pressure, they are maximally spready apart (i.e. in rarefaction). The distance that a full cycle of this wave occupies is the wavelength, λ, and the amount of time that a complete cycle is achieved is the period, T. Frequency is the inverse of the period

defined as the number of cycles per second, measured in hertz. Frequencies detectable by the human ear is within 20-20,0000 Hz; ultrasonic frequencies lie above this range.

Transducer Devices

For both diagnostic and therapeutic applications, ultrasound waves are generated via applying an electric charge to piezoelectric crystals housed within the transducer, leading to a change in mechanical pressure causing them to vibrate. Imaging ultrasound differs from therapeutic ultrasound on the basis of certain parameters, namely intensity (watts/cm^2). As opposed to planar, collimated beams used in ultrasound imaging and physiotherapy equipment, FUS beams are characterized by a focal region with intensities 3-4 orders of magnitude higher than the surface of the transducer. This implies tissues outside the focal region do not experience the same effects as the tissue within [45].

FUS Beams can be generated in more than one way using transducer designs that differ in terms of beam-formation and steering [56]. The most simple and common technique, geometric focusing, uses single element, concave transducers, in which lens geometry and positioning determines the fixed location of the focal region. Electronic focusing uses phased array transducers comprised of multiple piezoelectric elements that each have their own signal amplitude and frequency. This feature begets the versality of this technique, which allows the focal region to be displaced in the axial or lateral directions without physically moving the transducer. Commercial medical systems use both of these methods, where geometric steering is for gross positioning and electronic steering is for precise targeting [57].

Driving frequency is a key parameter of HIFU transducer designs that affects focal region volume and depth of penetration, both which are crucial and need to be

tailored for each target region of the body. Lower frequencies are able to penetrate deeper into tissues and produce larger foci, and higher frequencies penetrate less but can create tighter, more precise foci [58].

Section 1-4: HIFU Field characterization

Multiple characterization tools and techniques exist that are used for regulatory and research purposes for focused ultrasound technology. These are used for spatially mapping the acoustic field of a FUS transducer in terms of either intensities or pressures. Furthermore, knowing characteristics such as the position of the focal zone in the axial direction, and dimensions of the focal zone (axial length, maximal radial diameter) is crucial towards safe and effective administration of FUS for clinical use [57].

Hydrophone

Acoustic fields from a FUS transducer can be quantified using hydrophone transducers, which can obtain discrete, high-resolution 3D quantitative values of localized acoustic pressure. The most common type are needle hydrophones containing polyvinylidene fluoride, a piezoelectric polymer [57]. Tests are performed in water (i.e. "free-field conditions") to allow the sound to propagate in a non-attenuating medium. To allow for precise, point-wise measurement, the hydrophone is mounted onto a 3D positioning system. An oscilloscope is used to measure the output waveform signals from the hydrophone. While this technique is the most common in the preclinical setting, transducer probes and positioning equipment are expensive and limited in availability, and needle probes must be handled very carefully due to cavitation-based

damage at high acoustic pressures [59, 60]. Moreover, scanning entire fields are very time consuming and can take up to half a day to complete.

Schlieren Imaging and Infrared Imaging

Qualitative techniques such are Schlieren Imaging and Infrared (IR) imaging are used to evaluate ultrasound fields in terms of pressure and temperature distributions respectively. Schlieren imaging provides real-time 2D projections of the sound field based on its effects on refracting light in a liquid medium [61, 62]. IR Thermography involves placing an IR camera facing a tissue mimicking phantom that acts as an absorbing medium of the sound beam [63, 64]. Both techniques however require expensive optical equipment.

Gel phantoms and Thermochromic Liquid Crystals

Gel phantoms play an important role in FUS transducer characterization and quality assurance and are used to verify transducer alignment, visualize focal zone geometry/location and monitor temperature rise [57]. Heat-sensitive albumin protein and thermochromic dyes alike have been incorporated into gel phantoms for characterizing focused ultrasound transducers as well as a variety of other thermal ablation devices (microwave, radiofrequency, cryoablation) [65-68]. These two types of phantoms are irreversible and designated for single use. Moreover, the process for preparing the phantoms can be technically demanding (e.g. getting correct albumin concentration, controlling temperature) and there are concerns when handling reagent material (e.g. carcinogenic risk when exposed to unpolymerized polyacrylamide).

Thermochromic Liquid Crystal Films

The thermochromic effect is based on cholesteric crystals that undergoes a shift in alignment (i.e. "pitch") when exposed to a specified range of temperatures. This alters the absorption and reflection of different wavelengths of the visible spectrum, leading to a change in color [69]. Thermochromic liquid crystal (TLC) can be encapsulated onto films, which are flexible, black polyester-based films that contain an encapsulated layer of cholesteric crystals. As the film approaches and progresses through its specified temperature range, the film changes to red, green, blue, and black again when the temperature goes beyond the specified range [70]. As the pitch of the crystals vary continuously with temperature, additional hues (e.g. orange, yellow, violet) in between the primary color can be observed. These films can be considered as partially dynamic sensing devices, as it is noted in the literature that the time response of these films are on the order of 10ms [71].

Thermochromic liquid crystals films are found in many devices that require surface temperature sensing for safety, functional, or debugging purposes [70, 72]. TLC films can be found on equipment in the industrial and medical fields (e.g. bioreactors, adhesive body thermometers) [73]. For ultrasound technologies specifically, TLC films have been studied for usage in quality assurance research for planar physiotherapy transducers [67]. Intensity-output of physiotherapy transducers need to be checked periodically to ensure they fall within a certain range. If outside the range (too high or low), this precludes the physiotherapy transducer to provide safe and optimal treatment. The QA methods works via the incident ultrasound beam being attenuated by the TLC film. This leads to conversion of acoustic energy into thermal energy, signified by color changes on the film.

Chapter 2: Project Overview / Proof of Concept Experiment

Section 2-1 Overview

This present study sought to examine whether thermochromic liquid crystal (TLC) films could be used as a low-cost, time-efficient technique of characterizing the focal region of FUS beams. TLC films were obtained from two manufacturers; the first group was a sample set of films (Educational Innovations Inc, Bethel, CT USA) used for initial testing that contained 3 unique temperature sensitivity ranges: 20-25°C, 25-30°C, 30-35°C. The 2nd set (Hallcrest, Glenview, IL USA) contained 7 films with the following sensitivity ranges: 20-25°C, 25-30°C, 29-33°C, 30-35°C, 35-36°C, 35-40°C, 40-45°C. Table 1 provides color-transition temperatures for the Hallcrest films (specifications from the first manufacturer were not available).

Sensitivity Range	Red Start	Green Start	Blue Start	Blue to Black	Degree of Bandwidth
20-25°C	20	21	25	41	5
25-30°C	25	26	30	44	5
29-33°C	29	30	33	50	4
30-35°C	30	31	35	46	5
35-36°C	35	35.2	36	49	1
35-40°C	35	36	40	49	5
40-45°C	40	41	45	52	5

Table 1: Hallcrest Film Types

A preliminary investigation using a planar physiotherapy transducer (Chattanooga Rehab Group, Dallas, TX, USA) was conducted to verify that the films could detect temperature changes by an ultrasound beam in a reproducible manner. Then two FUS transducers were evaluated with a more controlled set-up and technique outlined in Chapter 3. The 500 KHz transducer experiment is compared to a gel phantom technique, and the 3.57 MHz transducer is compared to the gold standard

hydrophone technique. Figure 1 summarizes the entire process in developing the characterization method.
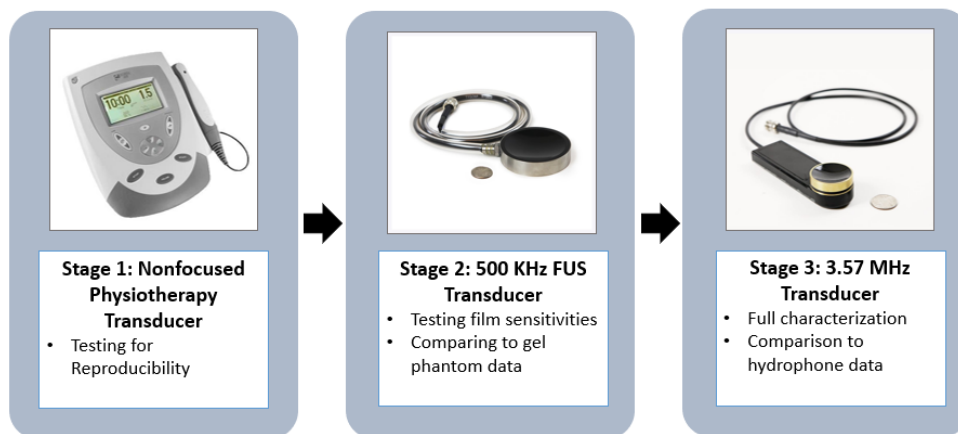
Figure 1: Project overview

Section 2-2 Proof-of-concept experimental setup

An initial verification test of the films was conducted using a non-focused, physiotherapy transducer. The TLC film was affixed to a foam window and the transducer was held in place centrally behind the film at a fixed distance using a ring stand. Figure 2 shows the submerged set-up in a plastic bin of non-degassed water. The transducer sonication parameters were set to a continuous 1 MHz wave output at an intensity of 2.0 W/cm^2. An images directly in front of the film was taken (iPhone XR) 2 seconds after powering on the transducer, which is the approximate time it took for the signal change on the film to stabilize. This experiment was repeated 5 times and images were then analyzed in Image J for cross-sectional area.
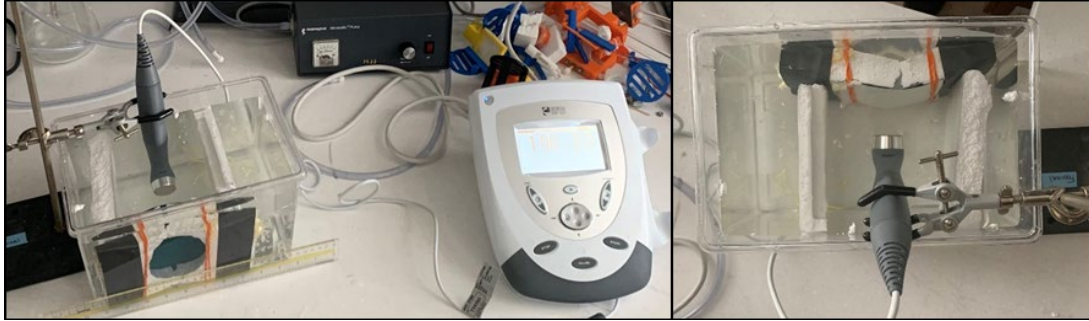
Figure 2: Proof of concept experiment using physiotherapy transducer.
(Left) Transducer facing TLC film sample. (right) Top-down view

Section 2-3: Results

Figure 3 shows the film facing the powered on transducer, which contained a darker area depicting the cross-sectional profile of the collimated ultrasound beam. All 5 images showed the same result and cross-sectional areas were calculated using the Image J freehand oval tool. The average area was 194.9 mm^2 +/- a standard deviation of 4.0, shown in Table 2. This experiment validated the temperature sensing effect of the film and allowed progression of the project into testing the FUS transducers.

Figure 3: Signal on TLC film (right: using ImageJ to find area of selection)

Trial #	Area (mm^2)
1	195.47
2	201.16
3	195.15
4	192.10
5	190.74
Average	194.923
Standard Deviation	4.021

Table 2: Area of Film signal

Chapter 3: TLC Film Characterization Method

Section 3-1: Introduction and Workflow

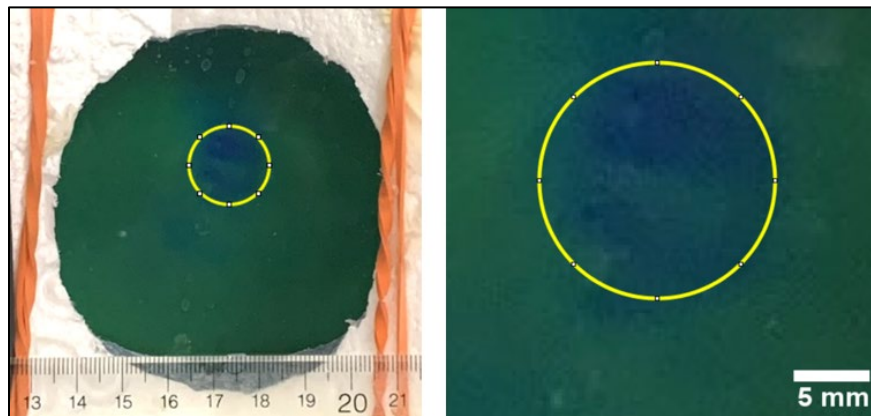After the previous experiment verified reproducible signals, proceeding experiments were conducted with two spherical, single element FUS transducers; one rated at a center frequency of 500 KHz (Sonic concepts, Bothell, WA, USA) and the other at 3.57 MHz (Sonic concepts, Bothell, WA, USA). The overall workflow (Figure 4) involves testing the film ranges against the two transducers to obtain images of the films, then processing them in Image J to obtain area measurements. These area measurements are plotted with respect to distance between the transducer and film.

Focal region dimensions are then interpolated from these plots. In both 500 KHz and 3.57 MHz experiments, distance between transducer and center of the focal zone (i.e. depth) are obtained. Additionally, axial length of the focal zone is determined by the 3.57 MHz transducer experiments by calculating -3dB and -6dB ranges (section 5-2).
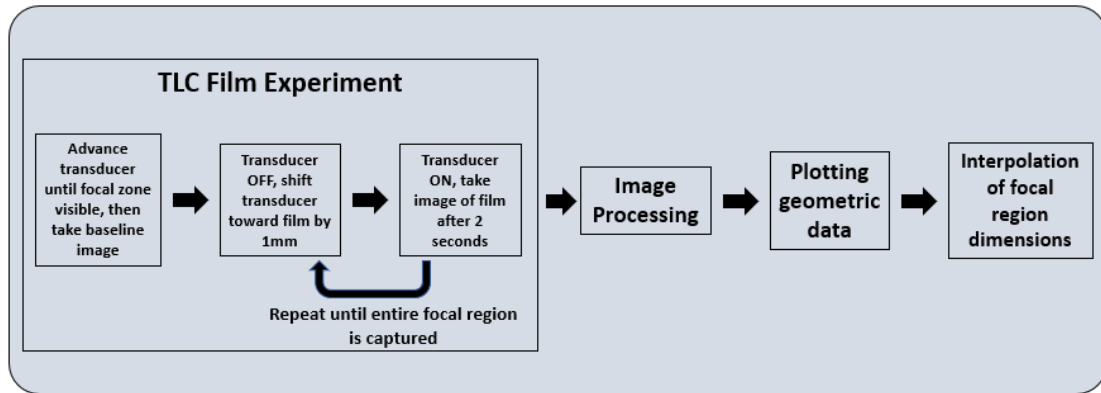
Figure 4: Workflow for TLC Film Characterization

Section 3-2: Test Set-up

Figure 5 shows the general water-tank setup for the FUS transducer experiments. The tank (51 cm × 27 cm × 32 cm), filled with deionized water, contained the submerged FUS transducer, which was attached to an aluminum alloy positioning system (Velmex, Bloomfield, NY, USA). This custom fixture provides translational movements in the x, y and z directions at a resolution of 1 mm. The TLC film is affixed to a 3D printed holder (Makexyz, Austin, TX, USA) that is fixed in place to the edges of the water tank.

Figure 5: Set up for 500KHz and 3.57MHz transducer experiments. Schematic (T: Transducer, F: TLC Film, C: Camera.

Section 3-3: TLC Experimental Procedure

First, the water temperature is taken using a thermal probe and recorded. The experiment begins with the transducer at a far distance away from the film, such that the focal zone is not intersecting the film. The transducer is powered on, then moved toward the TLC film using the aligner in 1mm increments. When a signal is detected on the film, an image is ta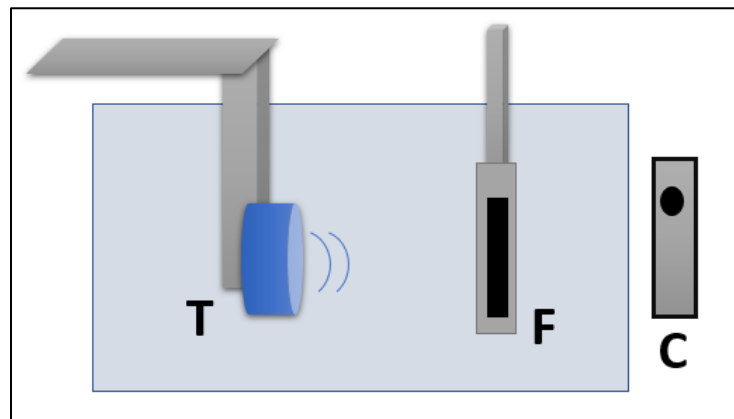ken, then the transducer is powered off. The transducer is positioned forward again, then powered on again. After ~2 seconds, another image of the film is obtained. The duration was chosen based off preliminary experiments that determined the minimal amount of time for the signal to stabilize on the film. This process is repeated until the film captures all 1mm sections of the focal zone. For each transducer, voltage and power settings were varied to examine variations of the characterization technique.

Section 3-4: Image Processing and Data Plotting

After conducting the TLC film experiments, image data is then processed through ImageJ software (ImageJ v1.52n, NIH, Bethesda, MD) to obtain geometric measurements of the focal zone in cross-sections capture by the TLC film. This data is then compared to results from two other characterization methods. Experiments from the 3.57 MHz transducer is compared to acoustic field data from a needle hydrophone experiment. Data from the 500 KHz transducer experiments is compared to a measurement (distance from transducer to center of focal zone i.e. focal depth) obtained from a previous study from the lab using the same transducer on a polyacrylamide gel phantom [74].

Figure 6 outlines the processing steps in Image J. First, the pixel-to-millimeter scaling was set according to a segment of ruler tape located on the 3D printed holder. A color thresholding filter was then applied to isolate the area of the signal from the background (Figure 6B). The area was then selected using the 'magic wand' tool and subsequent measurements for the area, perimeter, and major and minor axes were obtained using a best-fit ellipsoid approximation (Figure 6C).
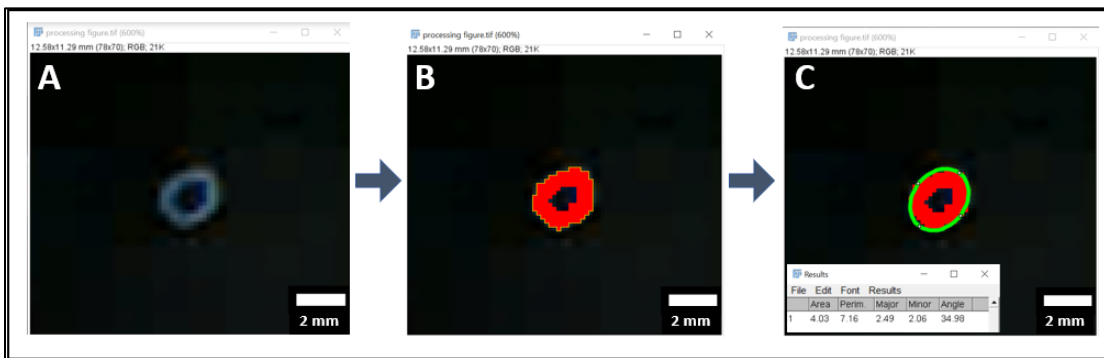
Figure 6: Image Processing for TLC film images. A) original image zoomed in; scaling established using ruler tape on 3D part. B) application of color thresholding filter and selection with magic wand tool (accounts for ALL area within the selection). C) Using ImageJ measuring tool through an ellipsoid approximation

Geometric data from the axial images of the focal zone were then input into Excel. Data from the experiments were organized by transducer type, film sensitivity that was tested, and function generator parameters (i.e. watts in the case of the 500 KHz transducer). Plots of transducer-film distance on the x-axis with corresponding values of cross-sectional areas of the signal on the y-axis were obtained. General trendlines for each plot using the $5^{th}, 6^{th}$ order polynomial function on Excel were generated. For comparison of the TLC film data with the hydrophone experiment for the 3.57 MHz transducer, these trendlines were used to calculate -3dB and -6dB ranges of the axial length of the focal zone. -3dB corresponds to 50% of the maximal cross-sectional area

calculated from the TLC imaging experiment, which was assumed to be at the center of the focal region in the axial dimension (i.e. where acoustic intensity is at a maximum). The -6dB corresponds to 25% of the maximal cross-sectional area.

Chapter 4: Validation with 500 KHz FUS Transducer
Section 4-1: 500 KHz Transducer Experimental Setup

The next set of experiments was conducted using an updated set-up with the 500 MHz FUS transducer (Figure 7). This specific transducer is driven by a combined function generator/acoustic amplifier (TPO-102, Sonic Concepts, Bothell WA, USA) via a 50 Ohm impedance matching circuit. The function generator contains controls for varying power (up to 150 W), the pulse width of the waveform (range 10 μ-seconds to 1 second), the pulse repetition frequency (range 1 kHz to 0.1 Hz, and exposure duration at increments of 0.1 seconds. 3 individual film sensitivities were tested: 20-25°C at 1.0W and 1.5W; 25-30°C at 1.5W, 2.0W, 2.5W, and 30-35°C at 2.0W, 2.5W, and 3.0W.
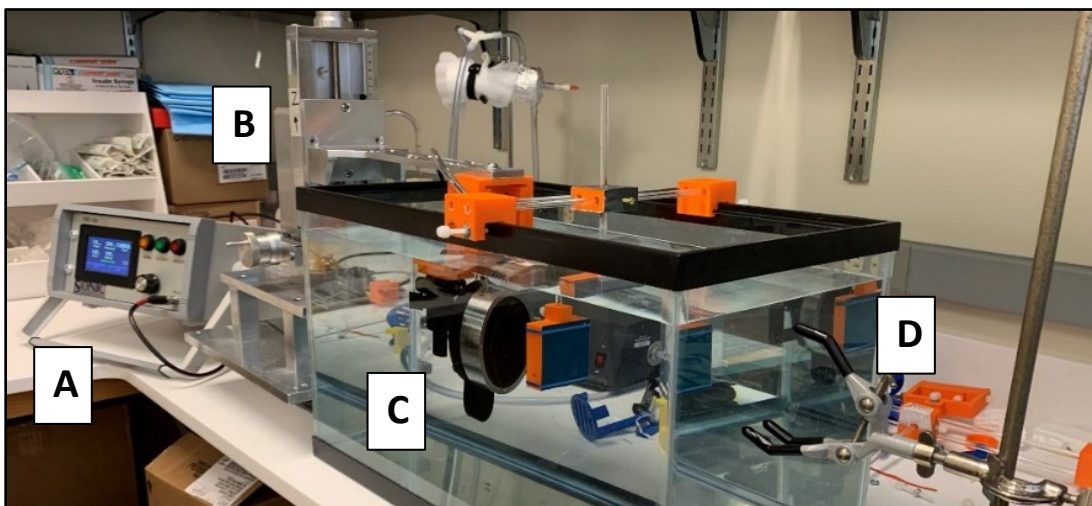

Figure 7: Set-up for 500 KHz Transducer experiments. A) Function generator; B) XYZ aligner; C) Transducer and TLC Film Holder; D) Camera holder

Section 4-2: TLC Film Results

Testing the first sample film (20-25°C) yielded film images that were highly variable and could not reliably recreate the Gaussian distribution associated with the focal zone geometry. It was also noted that the temperature of the water was 22°C and the film was green at baseline (Supplemental Figure 18), which may have had an effect on obtaining the cross-sectional snapshot of the focal zone. Testing the second sample film (25-30°C) yielded more uniform distributions. Since this film range was outside of the measured water temperature of 22°C, images of the focal zone appeared clearer against a black background (Supplemental Figure 19). With the third sample film (30-35°C) test with the 500 KHz transducer, data points followed a clear gaussian trend (Figure 9). There were slight differences in maximum cross-sectional area measurement when holding power constant between the three films. For example, at 2 Watts, the 2nd film was 23.7 mm^2 while the 3rd was 22.3 mm^2 (Table 3)
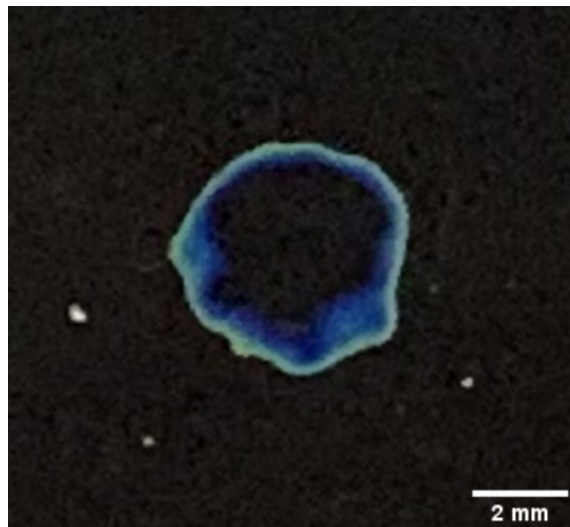

Figure 8: Cross section of the center of the focal region using (30-35°C) film
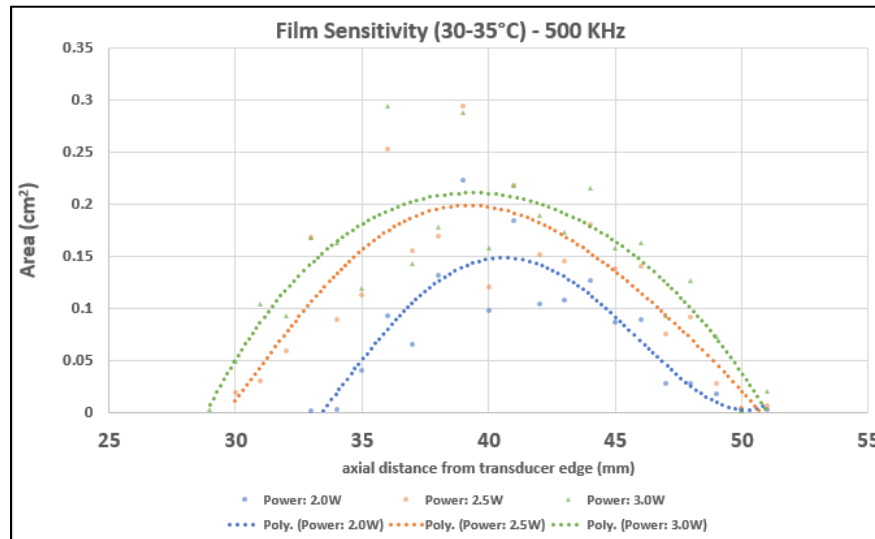
Figure 9: Plot of Transducer-Film distance vs Cross sectional area of TLC signal

Section 4-3: Comparison of 500 KHz Experiment with Gel Phantom Data

Table 3 summarizes key data from the TLC experiments with the 500 KHz transducer, including maximal cross sectional-area measured, and the distance between the transducer edge and film at which that data point was measured. The maximal cross-sectional area from each experiment was assumed to be located at the center of the focal zone (i.e. area of maximal intensity). This distance is compared to a previous experiment done by the lab that characterizes the focal region depth using a polyacrylamide phantom (Figure 10) [74]. Figure 10B shows the distance from the transducer edge to the center of the focal zone (14.1+26.57mm = 40.67mm). Note that as the film sensitivity range increased (i.e. from 20-25°C to 30-35°C), the deviation from the same measurement obtained from gel phantom data was smaller. This finding highlighted the importance of the film's temperature sensitivity.

Fig. 5 FUS transducer, coupling cone and water bolus: **b** Dimensions of the components, indicating the position of the focus. **a** Digital image of a thermal ablative lesion generated in a polyacrylamide phantom
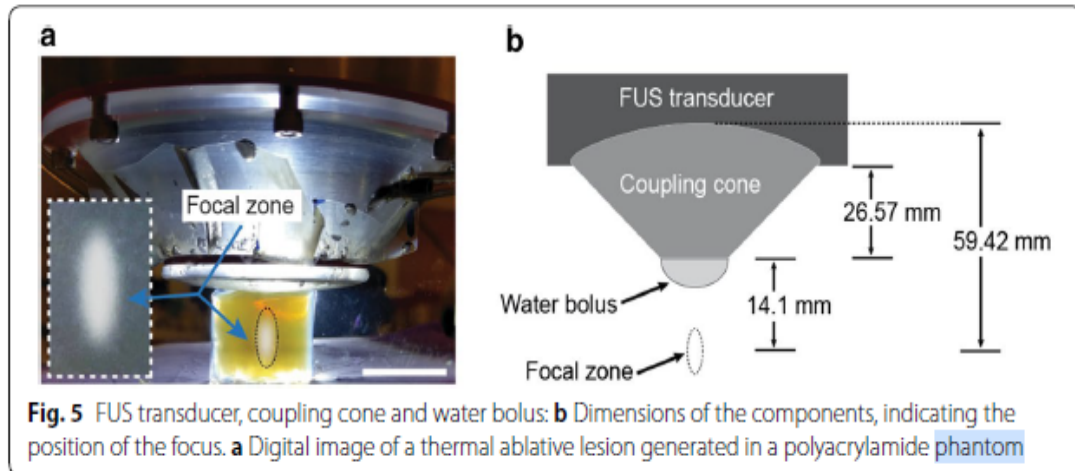
Figure 10: 500 KHz gel phantom data from previous paper in our lab [74]

Film Sensitivity	Watts	Maximal cross-sectional area	Depth i.e. Distance from transducer edge to film at maximal cross sectional – area	% Deviation from Gel Phantom data (40.67mm)
20-25°C	1.0	16.9 mm^2	35 mm	14%
	1.5	10.5 mm^2	37 mm	9.0%
25-30°C	1.5	11.9 mm^2	38 mm	6.6%
	2.0	23.7 mm^2	38 mm	6.6%
	2.5	32.8 mm^2	36 mm	11%
30-35°C	2.0	22.3 mm^2	39 mm	4.1%
	2.5	29.5 mm^2	39 mm	4.1%
	3.0	29.5 mm^2	39 mm	4.1%

Table 3: Comparing 500 KHz experiment data with gel-phantom experiment

Chapter 5: Validation with 3.57 MHz FUS Transducer

Section 5-1: 3.57 MHz Transducer Experimental Setup

The last set of experiments were conducted with the 3.57 MHz transducer, rated at a higher frequency than the previous transducer. The transducer is driven by a function generator (SDG2042X, Siglent, Solon, Ohio, USA) connected to a custom amplifier (AMP-200, Sonic Concepts, Bothell, WA, USA) via a 50 Ω impedance matching network. The transducer was powered with a continuous sine wave at 2V for 2 seconds, then an image of the film sensing the cross-section of the focal zone was obtained at each increment. 5 trials of one film (35-40°C) was tested at 2 volts peak-to-peak (experiments with the other 6 films were cancelled due to laboratory closing secondary to Covid-19 pandemic, see section 6-3 for future planning)

The final iteration of the characterization workflow was implemented for these experiments. An additional 3D printed component, designed to hold 35x25mm photoslide cassettes, was added to allow for rapid testing of the seven film sensitivities. Films were cut to approximately 40x40 mm squares and friction-fitted inside the photoslide cassette. These cassettes containing the film samples (Figure 11A) are then inserted into a slot within the holder component (Figure 11B). The holder has a viewing window for image capture (Figure 11C), allowing films to be quickly switched out for faster testing.
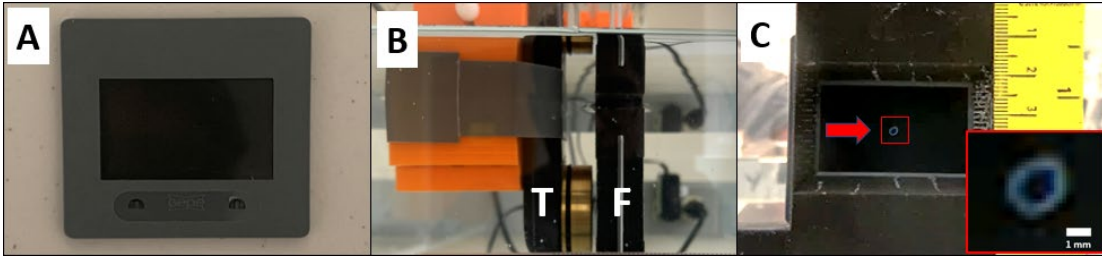
Figure 11: TLC Film Holder A) Film within photo slide cassette. B) Transducer (T) facing film holder (F). C) Image-capture view of film holder – inset cross section of focal zone zoomed in

Section 5-2: TLC Film Results

Figure 12 depicts results from one trial of the experiment with a trendline formed via polynomial approximation. The x-axis of the plot is the distance of the film from the transducer with its corresponding cross-sectional area (mm^2) of the focal zone sensed by the film on the y-axis. -3dB and -6dB ranges of the axial length of the focal zone are shown. The horizontal -3dB and -6dB lines are calculated (Table 4) by taking the range between the maximum and baseline areas, taking half (-3dB) or quarter (-6dB), then plotting on the chart. The x-values are then extrapolated by the intersection of the polynomial curve and the dB lines (downward arrows). The x-range (Table 4) approximates the axial length of the focal zone. Figure 13 averages all data points across the 5 experiments. Representative snapshots of the focal region are superimposed above the average areas at each distance.
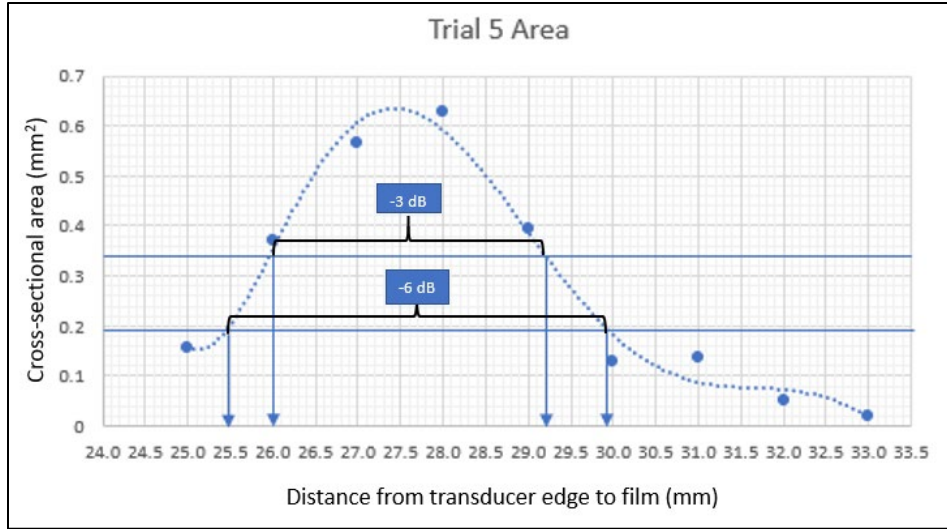
Figure 12: 3.57 MHz experiment with 35-40°C film, trial 5

dB range	3dB (.5)	6dB (.25)
y =	0.34	0.20
x range	3.2	4.4

Table 4: Obtaining -3dB and -6dB calculations for axial length of the focal zone
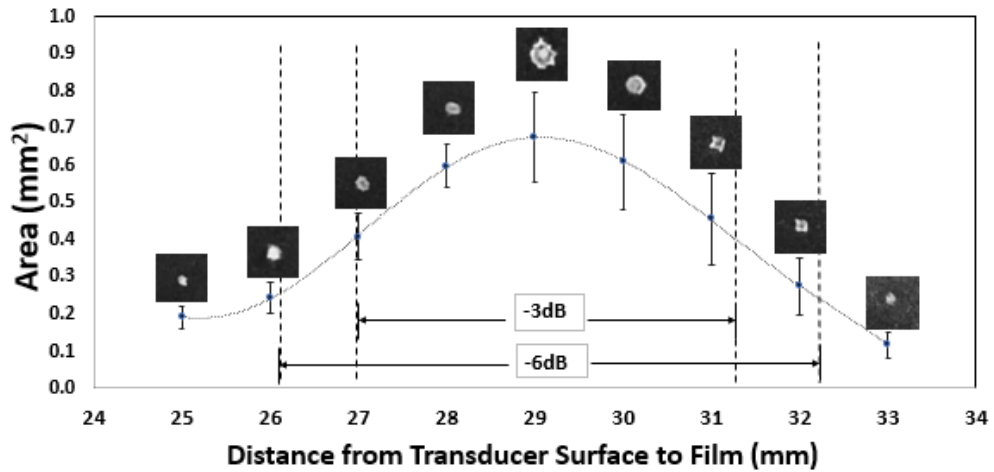
Figure 13: Averaged plot of TLC experiment with 3.57 MHz transducer (n=5)

Section 5-3: Hydrophone Experiment

Hydrophone measurements of the acoustic pressure field of the 3.57 MHz transducer was conducted to compare to the corresponding TLC film experiments in three trials. A needle hydrophone (Onda, Sunnyvale, CA, USA) operating in continuous mode was positioned in the tank using a 3D printed custom holder (LulzBot TAZ 5, Aleph Objects, CO). With the hydrophone fixed in place, the transducer was moved in all three dimensions (x, y, & z) in and around the focal zone using a step-size of 0.5 mm, while the measured voltage at each location was recorded using a digital oscilloscope (Tektronix SDG 2042X, Beaverton, OR, USA). Figure 14 is a schematic of the experimental components and Figure 15 is the actual setup.

Figure 14: Schematic of hydrophone experiments (T: transducer, H: Hydrophone)

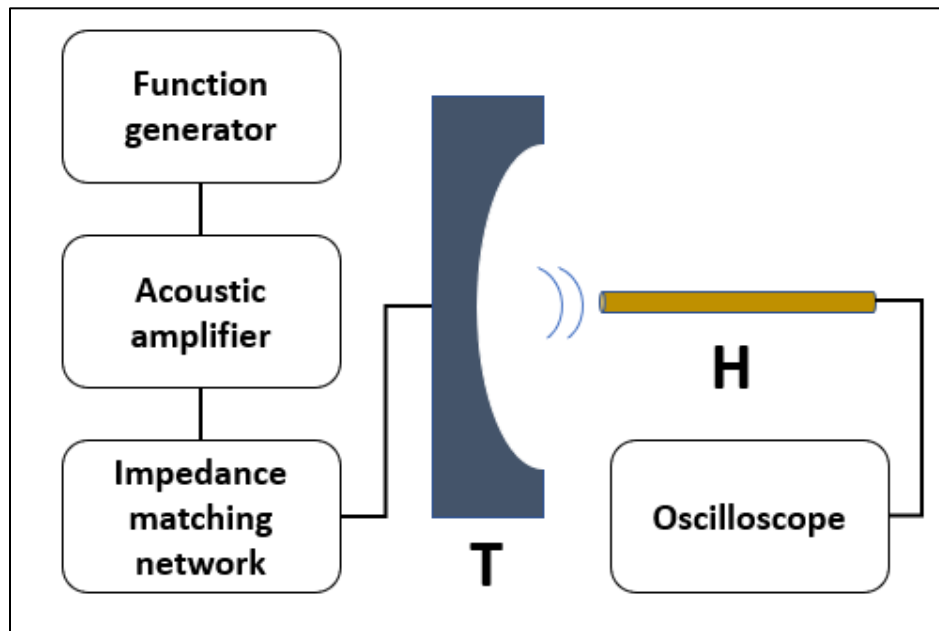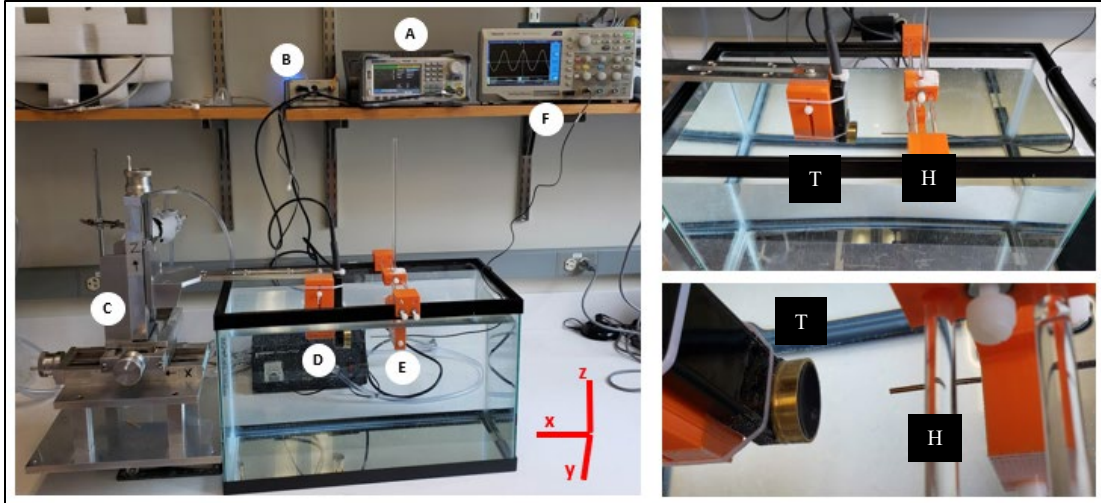**Figure 15: (left) hydrophone experiment with 3.57 MHz Transducer: A) function generator; B) amplifier; C) XYZ-positioning system; D) transducer; E needle hydrophone; F: Oscilloscope. (top-right) top-down view (T transducer; H Hydrophone); (bottom-right) closeup**

Section 5-4: Hydrophone Data

The center of the focal zone was designated as the location where the maximum pressure was recorded. This was found at 35 mm from the transducer surface. The values measured with the hydrophone were normalized to the maximum measured pressure at the center of the focal zone. The results for the width and length of the focal zone at -3 dB and -6 dB are shown in Figure 16. Figure 16A shows the focal width at -3 dB and -6 dB, interpolated from the measurements along the z-axis. Figure 16 B shows the focal length at -3 dB and -6 dB, interpolated from the measurements along the x-axis; Figure 16 C and D are schematic diagrams demonstrating dimensions and how the focal beam converges and diverges.
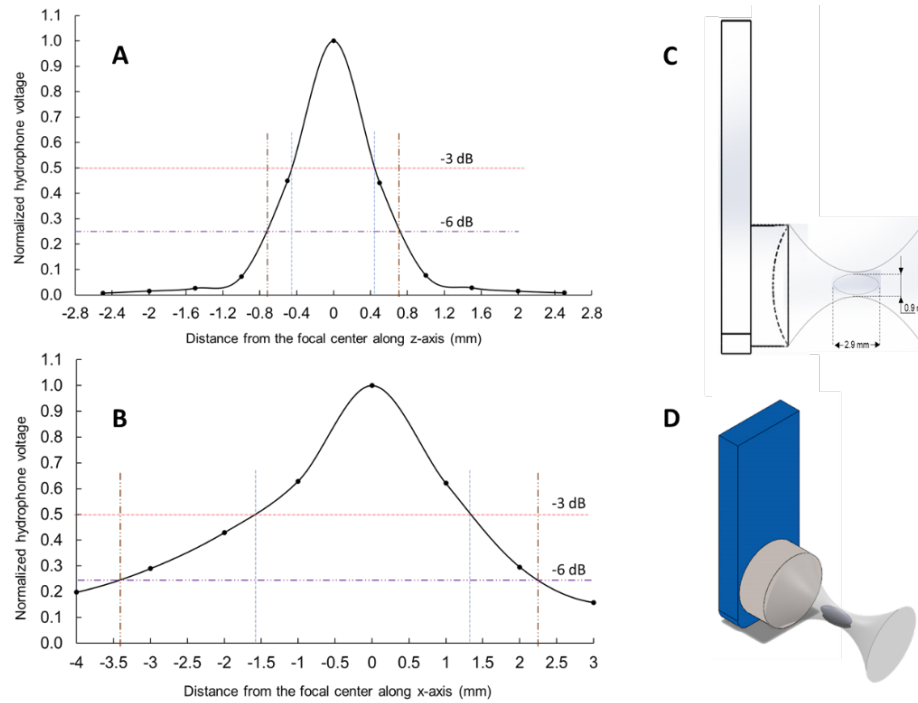
Figure 16: Hydrophone characterization results. A) Focal width (z-axis); B) Focal length (x-axis); C, D) 2D and 3D schematics of focal zone

Section 5-5: Comparison of 3.57 Transducer Experiment with Hydrophone Data

For the TLC experiments, axial lengths were calculated from each experiment then averaged. It was found that the TLC images were not able to provide a Gaussian curve for radial width which is required for -3 dB and -6 dB calculations – this could be due to the TLC film technique only being able to display the focal zone in the axial direction (i.e. the film was only utilized in one dimension); therefore an asterisk is placed within Table 5 to signify this could not be measured with the current experimental technique. Compared to the hydrophone measurements, the axial length of the focal zone from the TLC film experiments were 17% larger and 12% (-6 dB) smaller for the -3dB and -6dB ranges, respectively.

	-3 dB		-6 dB		D$_{H/F}$ (mm)
	Radial (mm)	Axial (mm)	Radial (mm)	Axial (mm)	
Hydrophone	0.9	2.9	1.5	5.7	35
TLC Film	*	3.5	*	5.0	34
% Disparity	-	19	-	19	2.9

Table 5: Comparison of focal zone Radial Diameter and Axial Length between hydrophone and TLC film data. (* signifies the technique is not able to provide radial dimensions in -3 dB and -6dB). D$_{H/F}$=Distance between transducer surface to focal center.

Section 5-6: Statistical Analysis

A nonparametric, two-sided Mann Whitney U test was employed to evaluate the degree of difference in two of the characteristic dimensions, specifically axial length (in -3 and -6 dB) and distance to the center of the focal region using the R programming language. (R Foundation for Statistical Computing, Vienna, Austria) . The three hydrophone experiment trials were compared to the 3 median results of the 5 TLC film trials. The null hypothesis (Ho) stated the two techniques were equal, while the alternative (Ha) stated them to be unequal. At a significance level of .05, p-values for the -3dB, -6dB axial lengths and distance to the focal center, were .12, 1.0, and .19 respectively, thus failing to reject the null hypothesis for the statistical comparisons and showing general agreement between the two characterization techniques.

Axial Length	Hydrophone (mm)	TLC Film (mm)
-3 dB	2.4	3.2
	2.7	3.4
	3.2	4.2
-6 dB	4.0	4.1
	4.2	4.0
	4.8	5.0
$D_{H/F}$ (mm)	34	35
	34	35
	35	35

Table 6: Data used for Mann Whitney U-Test. $D_{H/F}$=Distance between transducer surface to focal center.

Chapter 6: Discussion

Section 6.1 Analysis

In summary, we hypothesized that TLC films alone can be used to detect characteristic dimensions of HIFU focal regions that are critical in treatment planning. An initial test with a planar physiotherapy transducer verified visualization of an ultrasound field. The goal of the study was to develop a standardized, affordable method of using TLC films for FUS transducer quality assurance that can be easily implemented in any setting. Our technique consists of an interchangeable 3D printed component that allows testing of multiple TLC films, quick visualization of the focal zone, and a basic image processing algorithm to obtain geometric data. Results from the 3.57 MHz experiment were compared to the gold standard technique using an acoustic hydrophone, while that of the 500 KHz experiment compared to data from a previous study using the same transducer but with polyacrylamide gel phantoms, another common quality assurance method.

Focal depth (i.e. distance from the edge of the transducer to the center of the focal zone) were similar between TLC results and gel phantom images by Anastasiadis

et al. [74]. Percent deviation ranged from 11% to 4.1%, with the film sensitivity range of 30-35°C having the least deviation. This same dimension was also compared in the 3.57 MHz experiments to hydrophone data (29mm vs 35mm respectively), which had a 2.9% difference.

Knowing axial length of the focal zone is crucial for knowing how large the focal zone is in order to safely target tissues for ablative therapies or low-intensity applications. Results comparing axial lengths showed TLC films were 17% larger in the -3dB range and 12% smaller in the -6 dB range compared to hydrophone. This finding however is based on 5 trials at one voltage setting and with one temperature sensitivity range (35-40°C). Future experiments using more voltages and all seven film types will be conducted.

Section 6.2 Limitations

Limitations were encountered during the study related to the TLC film material and experimental protocol which will be discussed in this section. As shown with the preliminary experiments and with one of the films during the 500KHz experiment, **temperature of the water** bath will affect TLC film readouts, especially if the water temperature is within the sensitivity range of the film. Future experimental set-ups will include a temperature control to establish a uniform temperature and control for water temperature between experiments.
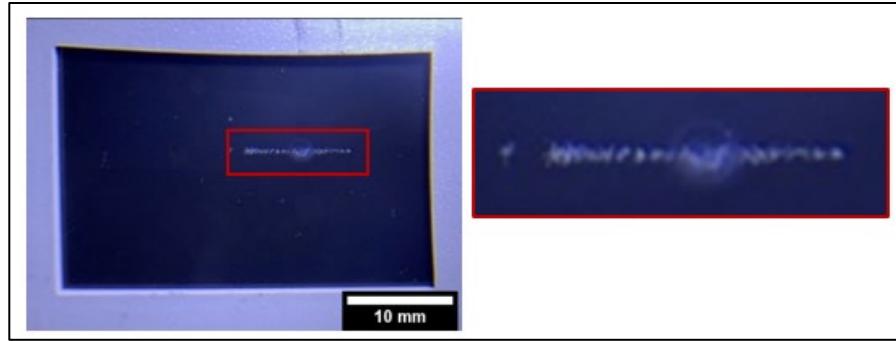
Figure 17: Film Degradation (inside red rectangle)

Re-use of the films may only be possible when powering the transducer at low voltages. A few experiments left irreversible markings on the film after higher voltages were tested. Figure 17 shows the film after powering the 3.57 MHz transducer at 6 volts peak-to-peak.

The process of manual image capture and image processing is **fairly labor intensive.** Future modification could include an attached, submersible module containing a camera circuit that collects the images of the film during the experiment, processes them in real-time and constructs a 3D representation of the focal zone. These changes would simplify the labor-intensive process and enable rapid quality testing of multiple FUS transducers.

Section 6-3: Future Experiments Plan

Due to the project being halted by the COVID-19 pandemic, future experiments are planned when access to the lab-setting is granted:

- Resume testing of 3.57 MHz Transducer experiments using all 7 film sensitivities and peak-to-peak voltages ranging from 1.5 – 3 Vpp

- Hydrophone experiments with 500 KHz Transducer so that film data can be compared to this standard technique.

- Polyacrylamide gel phantom experiments with the 3.57 MHZ transducer to compare TLC data to this technique.

- Temperature – Color calibration experiment with TLC films: This will entail experiments where the film is submerged in a temperature-controlled water bath (Figure 17). Images of the film are taken knowing the exposed temperature which will allow the ability of building an in-house temperature/color standard for all the films. This will help with calculating thermal gradients in the radial direction when conducting TLC film experiments.

The higher frequency transducer (3.57 MHz) gave limited visual output in terms of color gradients, simply because the rated focal zone is so small (on the order of 1mm). As a result, the TLC technique was not able to obtain radial widths in -3 dB and -6dB with the 3.57 MHz transducer. A transducer with a relatively lower frequency produces a larger foci with a detectable color gradient, which was observed during the experiments with the 500 KHz transducer. Given that a gradient of different colors, and therefore a gradient of temperatures could be generated, this can be used to calculate relative intensities, using the equation in Figure 18 and data obtained from film calibration experiments planned for the future. The relative intensities can thus be expressed as a gaussian distribution across the radial dimension of the focal zone, providing another characterization parameter similar to the hydrophone technique [58].
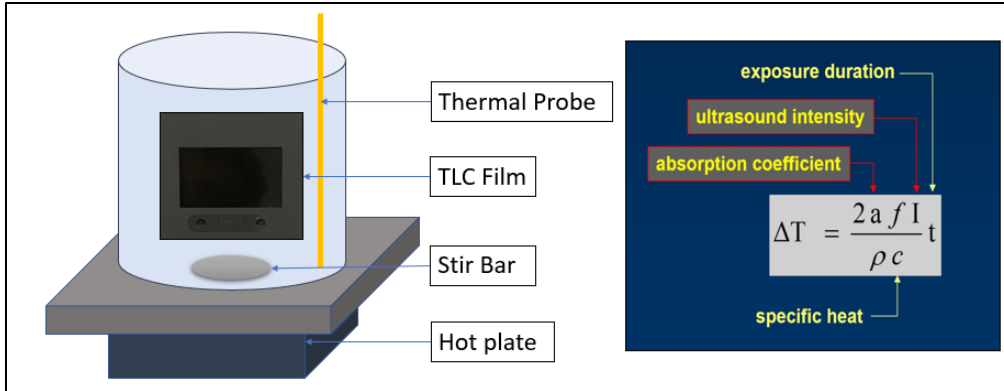
Figure 18: Future work. Right: TLC film calibration experiment; Left: Relationship between temperature change and intensity of ultrasound

Conclusion

FUS is gaining appeal over other treatment modalities (radiation, surgical excision, whole-body/systemic therapy) for a multitude of reasons: it is non-invasive (incisionless), targeted, treatments parameters are easily modifiable, and there are minimal off-target effects. Knowing characteristic dimensions of the focal region is crucial. Conventionally, hydrophones are used in measuring the width and length of the focal region. Accurate hydrophones are usually expensive and vulnerable to damage in the high magnitude of focused ultrasound. They also require precise setup and collect spot-size data which are labor-intensive and time-consuming procedures.

In this study, we present for the first time the use of TLC films for characterizing the focal zone of a FUS transducer. Results comparing to two other characterization techniques (needle hydrophone and gel phantoms) showed general agreement in a number of focal region dimensions, showing the viability of this method and potential for further improvement.

Supplementary Section

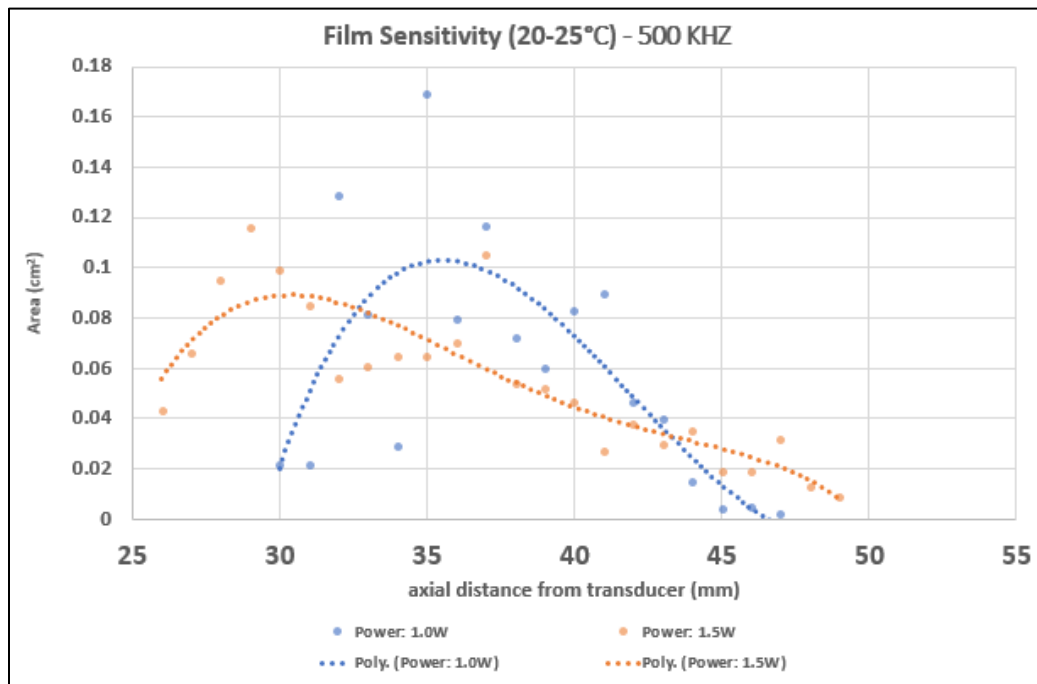## Section S-1: 500 KHz Transducer Data + Figures
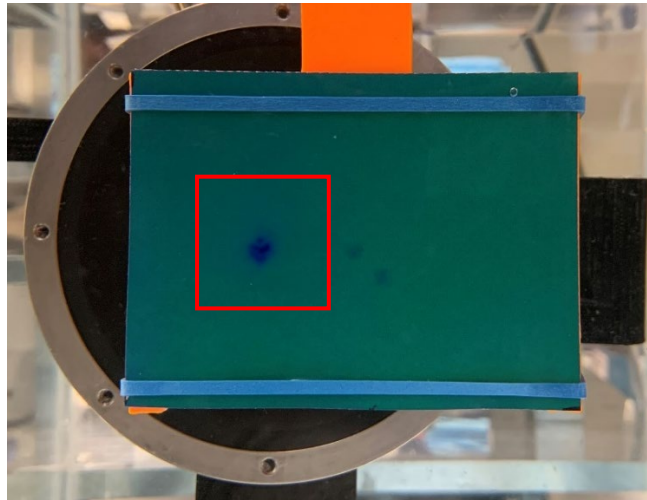
Figure 19: 500 KHz experiment with 20-25°C film Top: center of focal region in red box; Bottom: plot with polynomial approximations
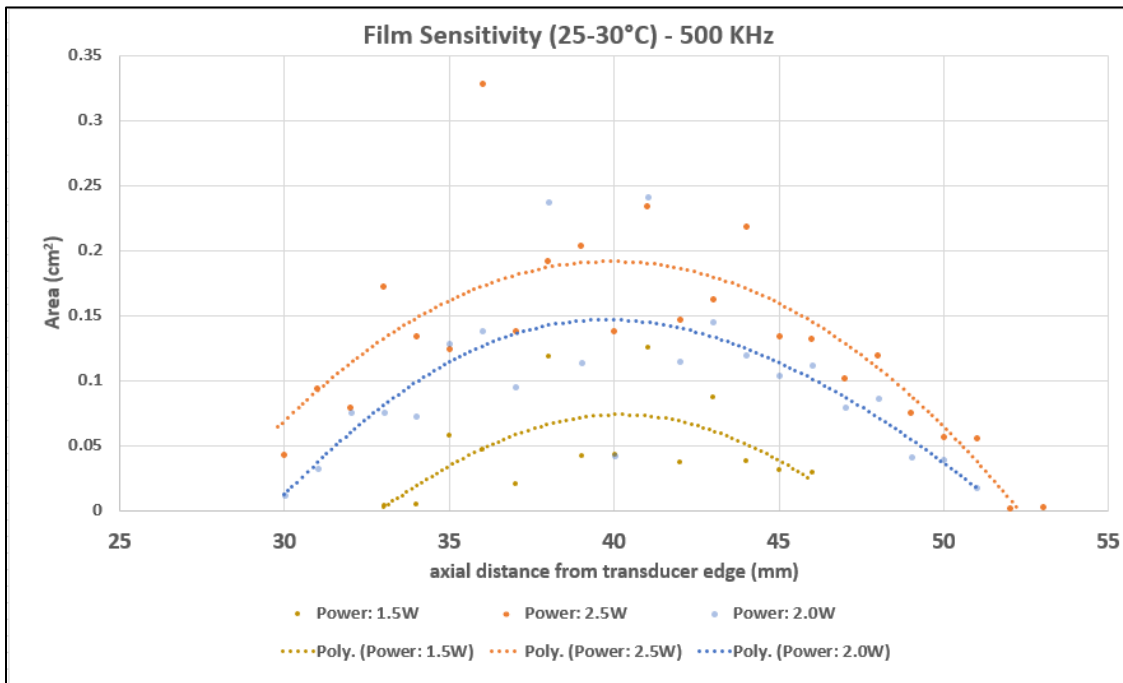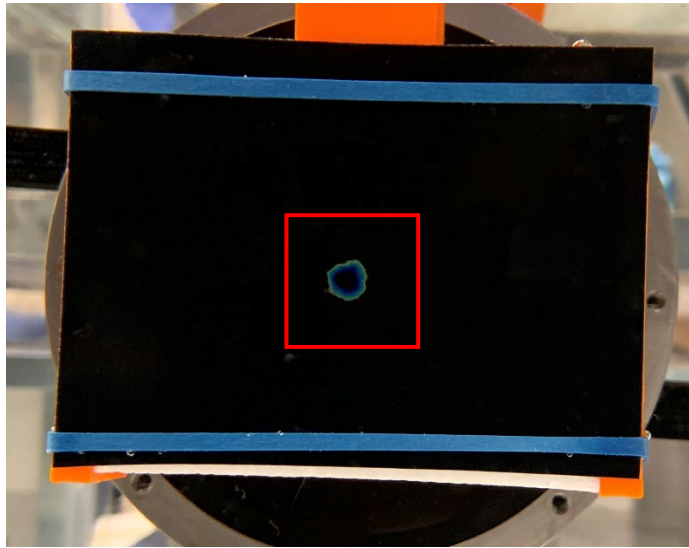
Figure 20: 500 KHz experiment with 25-30°C film. Top: center of focal region in red box; Bottom: plot with polynomial approximations

Section S-2 3.57 MHz Transducer Data + Figures
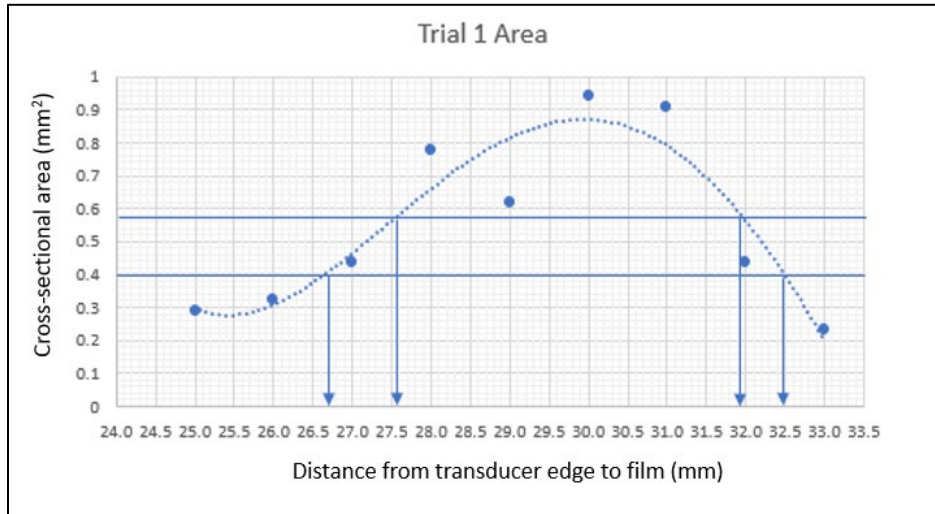
dB range	3dB (.5)	6dB (.25)
y =	0.588	0.41
x range =	4.3	5.8

Figure 21: 3.57 MHz experiment with 35-40°C film, trial 1 (top: plot with -3dB, -6dB lines; bottom: dB calculations)
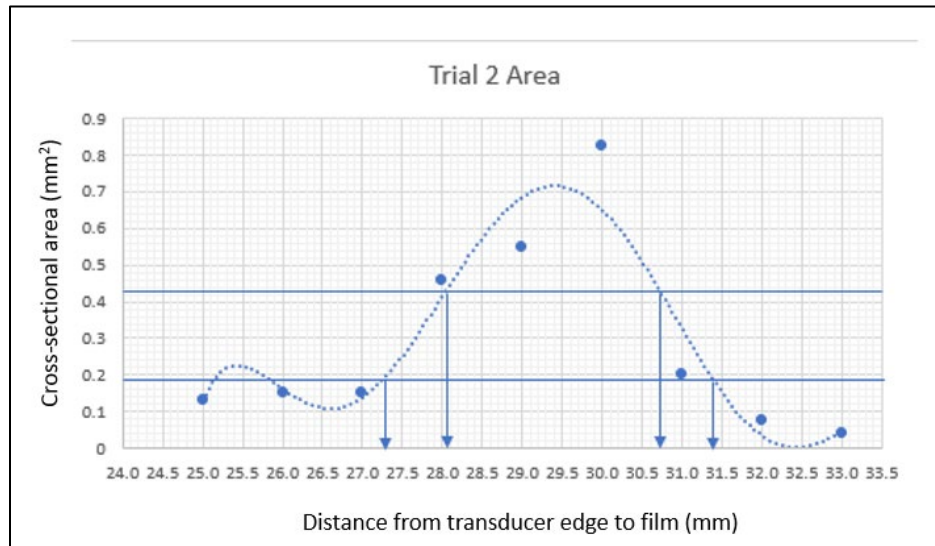
dB range	3dB (.5)	6dB (.25)
y =	0.43	0.20
x range	2.6	4.1
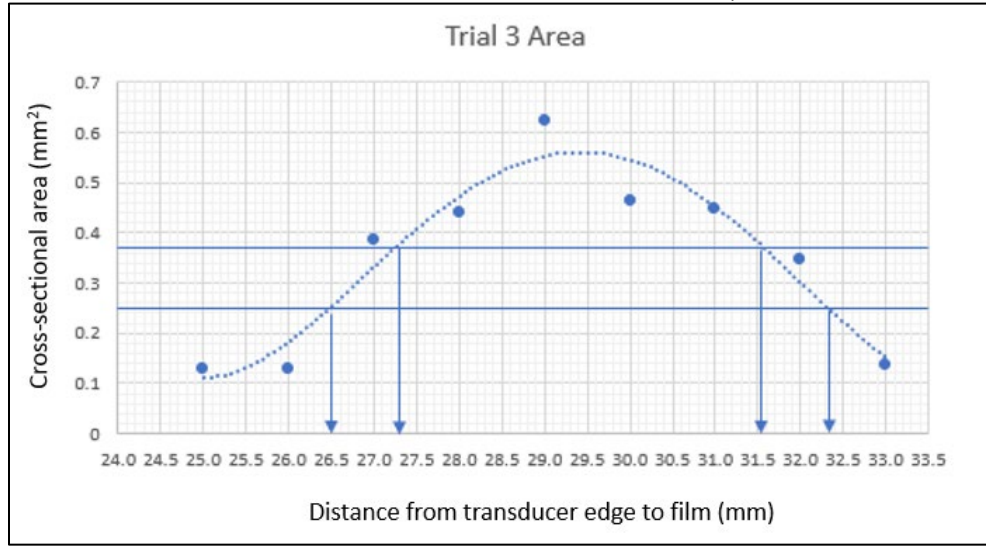
dB range	3dB (.5)	6dB (.25)
y =	0.38	0.25
x range	4.2	5.8

Figure 23: 3.57 MHz experiment with 35-40°C film, trial 3 (top: plot with -3dB, -6dB lines; bottom: dB calculations)
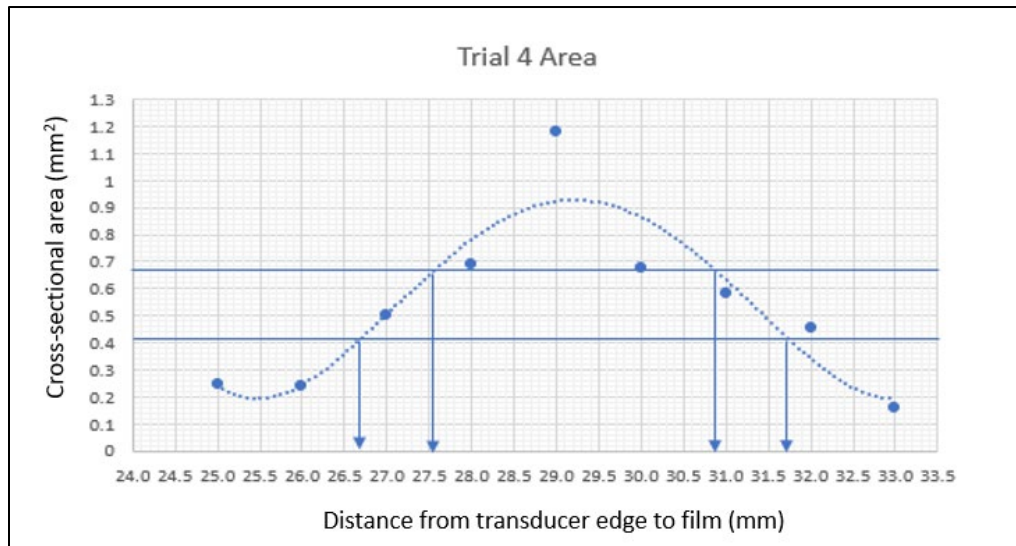
dB range	3dB (.5)	6dB (.25)
y =	0.67	0.41
x range	3.4	5

Figure 24: 3.57 MHz experiment with 35-40°C film, trial 4 (top: plot with -3dB, -6dB lines; bottom: dB calculations

Bibliography

[1] O'Brien, W. D., Jr. (2007) Ultrasound-biophysics mechanisms, *Prog Biophys Mol Biol 93*, 212-255.

[2] Willocks, J., Donald, I., Duggan, T. C., and Day, N. (1964) Foetal Cephalometry by Ultrasound, *J Obstet Gynaecol Br Commonw 71*, 11-20.

[3] Katzir, S. (2012) Who knew piezoelectricity? Rutherford and Langevin on submarine detection and the invention of sonar, *Notes and Records of the Royal Society 66*, 141-157.

[4] Fyfe, M. C., and Bullock, M. I. (1985) Therapeutic Ultrasound: Some Historical Background and Development in Knowledge of its Effect on Healing, *Australian Journal of Physiotherapy 31*, 220-224.

[5] Lynn, J. G., Zwemer, R. L., Chick, A. J., and Miller, A. E. (1942) A New Method for the Generation and Use of Focused Ultrasound in Experimental Biology, *J Gen Physiol 26*, 179-193.

[6] Fry, W. J., Mosberg, W. H., Jr., Barnard, J. W., and Fry, F. J. (1954) Production of focal destructive lesions in the central nervous system with ultrasound, *J Neurosurg 11*, 471-478.

[7] Guthkelch, A. N., Carter, L. P., Cassady, J. R., Hynynen, K. H., Iacono, R. P., Johnson, P. C., Obbens, E. A., Roemer, R. B., Seeger, J. F., Shimm, D. S., and et al. (1991) Treatment of malignant brain tumors with focused ultrasound hyperthermia and radiation: results of a phase I trial, *J Neurooncol 10*, 271-284.

[8] Sanghvi, N. T., Foster, R. S., Bihrle, R., Casey, R., Uchida, T., Phillips, M. H., Syrus, J., Zaitsev, A. V., Marich, K. W., and Fry, F. J. (1999) Noninvasive surgery of prostate tissue by high intensity focused ultrasound: an updated report, *Eur J Ultrasound 9*, 19-29.

[9] Hynynen, K., Colucci, V., Chung, A., and Jolesz, F. (1996) Noninvasive arterial occlusion using MRI-guided focused ultrasound, *Ultrasound in Medicine & Biology 22*, 1071-1077.

[10] Hynynen, K., and Jolesz, F. A. (1998) Demonstration of Potential Noninvasive Ultrasound Brain Therapy Through an Intact Skull, *Ultrasound in Medicine & Biology*.

[11] Cline, H. E., Hynynen, K., Hardy, C. J., Watkins, R. D., Schenck, J. F., and Jolesz, F. A. (1994) MR temperature mapping of focused ultrasound surgery, *Magnetic Resonance in Medicine 31*, 628-636.

[12] Rivens, I., Shaw, A., Civale, J., and Morris, H. (2007) Treatment monitoring and thermometry for therapeutic focused ultrasound, *Int J Hyperthermia 23*, 121-139.

[13] Wang, S., Zderic, V., and Frenkel, V. (2010) Extracorporeal, low-energy focused ultrasound for noninvasive and nondestructive targeted hyperthermia, *Future Oncol 6*, 1497-1511.

[14] Hersh, D. S., Kim, A. J., Winkles, J. A., Eisenberg, H. M., Woodworth, G. F., and Frenkel, V. (2016) Emerging Applications of Therapeutic Ultrasound in Neuro-oncology: Moving Beyond Tumor Ablation, *Neurosurgery 79*, 643-654.

[15] Elhelf, I. A. S., Albahar, H., Shah, U., Oto, A., Cressman, E., and Almekkawy, M. (2018) High intensity focused ultrasound: The fundamentals, clinical applications and research trends, *Diagnostic and Interventional Imaging 99*, 349-359.

[16] (2019) Focused Ultrasound Foundation State of the Field Report. URL: https://www.fusfoundation.org/news/state-of-the-field-report-2019-now-available.

[17] Elias, W. J., Huss, D., Voss, T., Loomba, J., Khaled, M., Zadicario, E., Frysinger, R. C., Sperling, S. A., Wylie, S., Monteith, S. J., Druzgal, J., Shah, B. B., Harrison, M., and Wintermark, M. (2013) A Pilot Study of Focused Ultrasound Thalamotomy for Essential Tremor, *New England Journal of Medicine 369*, 640-648.

[18] Yeo, S. Y., Elevelt, A., Donato, K., van Rietbergen, B., ter Hoeve, N. D., van Diest, P. J., and Grull, H. (2015) Bone metastasis treatment using magnetic resonance-guided high intensity focused ultrasound, *Bone 81*, 513-523.

[19] Gorny, K. R., Borah, B. J., Brown, D. L., Woodrum, D. A., Stewart, E. A., and Hesley, G. K. (2014) Incidence of Additional Treatments in Women Treated with MR-Guided Focused US for Symptomatic Uterine Fibroids: Review of 138 Patients with an Average Follow-up of 2.8 Years, *Journal of Vascular and Interventional Radiology 25*, 1506-1512.

[20] Merckel, L. G., Bartels, L. W., Kohler, M. O., van den Bongard, H. J. G. D., Deckers, R., Mali, W. P. T. M., Binkert, C. A., Moonen, C. T., Gilhuijs, K. G. A., and van den Bosch, M. A. A. J. (2013) MR-Guided High-Intensity Focused Ultrasound Ablation of Breast Cancer with a Dedicated Breast Platform, *Cardiovascular and Interventional Radiology 36*, 292-301.

[21] Zhu, L., Altman, M. B., Laszlo, A., Straube, W., Zoberi, I., Hallahan, D. E., and Chen, H. (2019) Ultrasound Hyperthermia Technology for Radiosensitization, *Ultrasound Med Biol 45*, 1025-1043.

[22] Krawczyk, P. M., Eppink, B., Essers, J., Stap, J., Rodermond, H., Odijk, H., Zelensky, A., van Bree, C., Stalpers, L. J., Buist, M. R., Soullie, T., Rens, J., Verhagen, H. J., O'Connor, M. J., Franken, N. A., Ten Hagen, T. L., Kanaar, R., and Aten, J. A. (2011) Mild hyperthermia inhibits homologous recombination, induces BRCA2 degradation, and sensitizes cancer cells to poly (ADP-ribose) polymerase-1 inhibition, *Proc Natl Acad Sci U S A 108*, 9851-9856.

[23] Dimcevski, G., Kotopoulis, S., Bjanes, T., Hoem, D., Schjott, J., Gjertsen, B. T., Biermann, M., Molven, A., Sorbye, H., McCormack, E., Postema, M., and Gilja, O. H. (2016) A human clinical trial using ultrasound and microbubbles to enhance gemcitabine treatment of inoperable pancreatic cancer, *J Control Release 243*, 172-181.

[24] Hancock, H. A., Smith, L. H., Cuesta, J., Durrani, A. K., Angstadt, M., Palmeri, M. L., Kimmel, E., and Frenkel, V. (2009) Investigations into pulsed high-intensity focused ultrasound-enhanced delivery: preliminary evidence for a novel mechanism, *Ultrasound Med Biol 35*, 1722-1736.

[25] Frenkel, V., Kimmel, E., and Iger, Y. (2000) Ultrasound-facilitated transport of silver chloride (AgCl) particles in fish skin, *J Control Release 68*, 251-261.

[26] Frenkel, V., Oberoi, J., Stone, M. J., Park, M., Deng, C., Wood, B. J., Neeman, Z., Horne, M., 3rd, and Li, K. C. (2006) Pulsed high-intensity focused ultrasound enhances thrombolysis in an in vitro model, *Radiology 239*, 86-93.

[27] Hynynen, K., McDannold, N., Vykhodtseva, N., and Jolesz, F. A. (2001) Noninvasive MR imaging-guided focal opening of the blood-brain barrier in rabbits, *Radiology 220*, 640-646.

[28] Huang, Y., Alkins, R., Schwartz, M. L., and Hynynen, K. (2017) Opening the Blood-Brain Barrier with MR Imaging-guided Focused Ultrasound: Preclinical Testing on a Trans-Human Skull Porcine Model, *Radiology 282*, 123-130.

[29] Marquet, F., Tung, Y. S., Teichert, T., Ferrera, V. P., and Konofagou, E. E. (2011) Noninvasive, transient and selective blood-brain barrier opening in non-human primates in vivo, *PLoS One 6*, e22598.

[30] Kinoshita, M., McDannold, N., Jolesz, F. A., and Hynynen, K. (2006) Noninvasive localized delivery of Herceptin to the mouse brain by MRI-guided focused ultrasound-induced blood-brain barrier disruption, *Proc Natl Acad Sci U S A 103*, 11719-11723.

[31] Aryal, M., Vykhodtseva, N., Zhang, Y. Z., Park, J., and McDannold, N. (2013) Multiple treatments with liposomal doxorubicin and ultrasound-induced disruption of blood-tumor and blood-brain barriers improve outcomes in a rat glioma model, *J Control Release 169*, 103-111.

[32] Wei, K. C., Chu, P. C., Wang, H. Y., Huang, C. Y., Chen, P. Y., Tsai, H. C., Lu, Y. J., Lee, P. Y., Tseng, I. C., Feng, L. Y., Hsu, P. W., Yen, T. C., and Liu, H. L. (2013) Focused ultrasound-induced blood-brain barrier opening to enhance temozolomide delivery for glioblastoma treatment: a preclinical study, *PLoS One 8*, e58995.

[33] Lipsman, N., Meng, Y., Bethune, A. J., Huang, Y., Lam, B., Masellis, M., Herrmann, N., Heyn, C., Aubert, I., Boutet, A., Smith, G. S., Hynynen, K., and Black, S. E. (2018) Blood-brain barrier opening in Alzheimer's disease using MR-guided focused ultrasound, *Nat Commun 9*, 2336.

[34] Mainprize, T., Lipsman, N., Huang, Y., Meng, Y., Bethune, A., Ironside, S., Heyn, C., Alkins, R., Trudeau, M., Sahgal, A., Perry, J., and Hynynen, K. (2019) Blood-Brain Barrier Opening in Primary Brain Tumors with Non-invasive MR-Guided Focused Ultrasound: A Clinical Safety and Feasibility Study, *Sci Rep 9*, 321.

[35] Abrahao, A., Meng, Y., Llinas, M., Huang, Y., Hamani, C., Mainprize, T., Aubert, I., Heyn, C., Black, S. E., Hynynen, K., Lipsman, N., and Zinman, L. (2019) First-in-human trial of blood–brain barrier opening in amyotrophic lateral sclerosis using MR-guided focused ultrasound, *Nature Communications 10*, 4373.

[36] Fry, F. J., Ades, H. W., and Fry, W. J. (1958) Production of reversible changes in the central nervous system by ultrasound, *Science (New York, N.Y.) 127*, 83-84.

[37] Sanguinetti, J. L., Hameroff, S., Smith, E. E., Sato, T., Daft, C. M. W., Tyler, W. J., and Allen, J. J. B. (2020) Transcranial Focused Ultrasound to the Right Prefrontal Cortex Improves Mood and Alters Functional Connectivity in Humans, *Front Hum Neurosci 14*, 52.

[38] Tufail, Y., Matyushov, A., Baldwin, N., Tauchmann, M. L., Georges, J., Yoshihiro, A., Tillery, S. I., and Tyler, W. J. (2010) Transcranial pulsed ultrasound stimulates intact brain circuits, *Neuron 66*, 681-694.

[39] Deffieux, T., Younan, Y., Wattiez, N., Tanter, M., Pouget, P., and Aubry, J. F. (2013) Low-intensity focused ultrasound modulates monkey visuomotor behavior, *Curr Biol 23*, 2430-2433.

[40] Kim, M. G., Kamimura, H. A. S., Lee, S. A., Aurup, C., Kwon, N., and Konofagou, E. E. (2020) Image-guided focused ultrasound modulates electrically evoked motor neuronal activity in the mouse peripheral nervous system in vivo, *J Neural Eng 17*, 026026.

[41] Juan, E. J., Gonzalez, R., Albors, G., Ward, M. P., and Irazoqui, P. (2014) Vagus Nerve Modulation Using Focused Pulsed Ultrasound: Potential Applications and Preliminary Observations in a Rat, *Int J Imaging Syst Technol 24*, 67-71.

[42] Downs, M. E., Lee, S. A., Yang, G., Kim, S., Wang, Q., and Konofagou, E. E. (2018) Non-invasive peripheral nerve stimulation via focused ultrasound in vivo, *Phys Med Biol 63*, 035011.

[43] Jiang, W., Wang, Y., Tang, J., Peng, J., Wang, Y., Guo, Q., Guo, Z., Li, P., Xiao, B., and Zhang, J. (2016) Low-intensity pulsed ultrasound treatment improved the rate of autograft peripheral nerve regeneration in rat, *Sci Rep 6*, 22773.

[44] Ezeokeke, C. K., Bobola, M. S., Selby, M., Ko, J. H., Friedly, J. L., and Mourad, P. D. (2020) Case study of an amputee regaining sensation and muscle function in a residual limb after peripheral nerve stimulation by intense focused ultrasound, *Brain Stimul 13*, 527-529.

[45] Frenkel, V. (2008) Ultrasound mediated delivery of drugs and genes to solid tumors, *Adv Drug Deliv Rev 60*, 1193-1208.

[46] Li, T., Wang, Y. N., Khokhlova, T. D., D'Andrea, S., Starr, F., Chen, H., McCune, J. S., Risler, L. J., Mashadi-Hossein, A., Hingorani, S. R., Chang, A., and Hwang, J. H. (2015) Pulsed High-Intensity Focused Ultrasound Enhances Delivery of Doxorubicin in a Preclinical Model of Pancreatic Cancer, *Cancer Res 75*, 3738-3746.

[47] Poff, J. A., Allen, C. T., Traughber, B., Colunga, A., Xie, J., Chen, Z., Wood, B. J., Van Waes, C., Li, K. C., and Frenkel, V. (2008) Pulsed high-intensity focused ultrasound enhances apoptosis and growth inhibition of squamous cell carcinoma xenografts with proteasome inhibitor bortezomib, *Radiology 248*, 485-491.

[48] Maxwell, A. D., Owens, G., Gurm, H. S., Ives, K., Myers, D. D., Jr., and Xu, Z. (2011) Noninvasive treatment of deep venous thrombosis using pulsed ultrasound cavitation therapy (histotripsy) in a porcine model, *J Vasc Interv Radiol 22*, 369-377.

[49] Abi-Jaoudeh, N., Pritchard, W. F., Amalou, H., Linguraru, M., Chiesa, O. A., Adams, J. D., Gacchina, C., Wesley, R., Maruvada, S., McDowell, B., Frenkel, V., Karanian, J. W., and Wood, B. J. (2012) Pulsed high-intensity-focused US and tissue plasminogen activator (TPA) versus TPA alone for thrombolysis of occluded bypass graft in swine, *J Vasc Interv Radiol 23*, 953-961 e952.

[50] Nazer, B., Ghahghaie, F., Kashima, R., Khokhlova, T., Perez, C., Crum, L., Matula, T., and Hata, A. (2015) Therapeutic Ultrasound Promotes Reperfusion and Angiogenesis in a Rat Model of Peripheral Arterial Disease, *Circ J 79*, 2043-2049.

[51] Siegel, R. J., Atar, S., Fishbein, M. C., Brasch, A. V., Peterson, T. M., Nagai, T., Pal, D., Nishioka, T., Chae, J. S., Birnbaum, Y., Zanelli, C., and Luo, H. (2001) Noninvasive transcutaneous low frequency ultrasound enhances thrombolysis in peripheral and coronary arteries, *Echocardiography 18*, 247-257.

[52] Leung, K. S., Lee, W. S., Tsui, H. F., Liu, P. P., and Cheung, W. H. (2004) Complex tibial fracture outcomes following treatment with low-intensity pulsed ultrasound, *Ultrasound Med Biol 30*, 389-395.

[53] Pounder, N. M., and Harrison, A. J. (2008) Low intensity pulsed ultrasound for fracture healing: a review of the clinical evidence and the associated biological mechanism of action, *Ultrasonics 48*, 330-338.

[54] Gold, M. H., Coleman Wp, I. V., Coleman W, III, and Weiss, R. (2019) A randomized, controlled multicenter study evaluating focused ultrasound treatment for fat reduction in the flanks, *J Cosmet Laser Ther 21*, 44-48.

[55] Suh, D. H., Shin, M. K., Lee, S. J., Rho, J. H., Lee, M. H., Kim, N. I., and Song, K. Y. (2011) Intense focused ultrasound tightening in Asian skin: clinical and pathologic results, *Dermatol Surg 37*, 1595-1602.

[56] Haar, G. T., and Coussios, C. (2007) High intensity focused ultrasound: physical principles and devices, *Int J Hyperthermia 23*, 89-104.

[57] Civale, J., Rivens, I., and ter Haar, G. (2015) Quality assurance for clinical high intensity focused ultrasound fields, *Int J Hyperthermia 31*, 193-202.

[58] Ellens, N. P., and Partanen, A. (2017) Preclinical MRI-Guided Focused Ultrasound: A Review of Systems and Current Practices, *IEEE Trans Ultrason Ferroelectr Freq Control 64*, 291-305.

[59] Zanelli, C. I., and Howard, S. M. (2006) A robust hydrophone for HIFU metrology, In *AIP Conference Proceedings*, pp 618-622, American Institute of Physics.

[60] Martin, K., and Fernandez, R. (1997) A thermal beam-shape phantom for ultrasound physiotherapy transducers, *Ultrasound Med Biol 23*, 1267-1274.

[61] Kudo, N., Ouchi, H., Yamamoto, K., and Sekimizu, H. (2004) A simple Schlieren system for visualizing a sound field of pulsed ultrasound, *Journal of Physics: Conference Series 1*, 146-149.

[62] Kremer, M., Caskey, C., and Grissom, W. (2015) Background-oriented schlieren imaging and tomography for rapid measurement of FUS pressure fields: initial results, *Journal of Therapeutic Ultrasound 3*.

[63] Gutierrez, M. I., Leija, L., and Vera, A. (2008) Therapy ultrasound equipment characterization: Comparison of three techniques, *Conf Proc IEEE Eng Med Biol Soc*.

[64] Shaw, A., and Nunn, J. (2010) The feasibility of an infrared system for real-time visualization and mapping of ultrasound fields, *Phys Med Biol 55*, N321-327.

[65] Dabbagh, A., Abdullah, B. J., Abu Kasim, N. H., and Ramasindarum, C. (2014) Reusable heat-sensitive phantom for precise estimation of thermal profile in hyperthermia application, *Int J Hyperthermia 30*, 66-74.

[66] Eranki, A., Mikhail, A. S., Negussie, A. H., Katti, P. S., Wood, B. J., and Partanen, A. (2019) Tissue-mimicking thermochromic phantom for characterization of HIFU devices and applications, *Int J Hyperthermia 36*, 518-529.

[67] Qureshi, F., Larrabee, Z., Roth, C., Hananel, A., Eames, M., Moore, D., Snell, J., Kassell, N., and Aubry, J.-F. (2015) Thermochromic phantom for therapeutic ultrasound daily quality assurance, *Journal of Therapeutic Ultrasound 3*.

[68] Menikou, G., and Damianou, C. (2017) Acoustic and thermal characterization of agar based phantoms used for evaluating focused ultrasound exposures, *J Ther Ultrasound 5*, 14.

[69] White, M. A., and LeBlanc, M. (1999) Thermochromism in Commercial Products, *Journal of Chemical Education 76*, 1201.

[70] Smith, C. R., Sabatino, D. R., and Praisner, T. J. (2001) Temperature sensing with thermochromic liquid crystals, *Experiments in Fluids 30*, 190-201.

[71] Orozco, G. A. L. M. a. G. A. V. (2009) *Three Dimensional Temperature Distribution Analysis of Ultrasound Therapy Equipments Using Thermochromic Liquid Crystal Films*, IntechOpen, Austria.

[72] Popov, N., Honaker, L. W., Popova, M., Usol'tseva, N., Mann, E. K., Jakli, A., and Popov, P. (2017) Thermotropic Liquid Crystal-Assisted Chemical and Biological Sensors, *Materials (Basel) 11*.

[73] Ashforth-Frost, S. (1996) Quantitative thermal imaging using liquid crystals, *J Biomed Opt 1*, 18-27.

[74] Anastasiadis, P., Mohammadabadi, A., Fishman, M. J., Smith, J. A., Nguyen, B. A., Hersh, D. S., and Frenkel, V. (2019) Design, characterization and evaluation of a laser-guided focused ultrasound system for preclinical investigations, *Biomed Eng Online 18*, 36.